

Gaussian decomposition of H I surveys

IV. Galactic intermediate- and high-velocity clouds

U. Haud

Tartu Observatory, 61 602 Tõravere, Tartumaa, Estonia
e-mail: urmas@aai.ee

Received November 1, 2018; accepted November 1, 2018

ABSTRACT

Context. Traditionally intermediate- (IVC) and high-velocity hydrogen clouds (HVC) were defined to be concentrations of H I gas, with line-of-sight velocities that are inconsistent with data on the differential rotation of the Galaxy.

Aims. We attempt to demonstrate that IVCs and HVCs can be identified from density enhancements in parameter distributions of Galactic H I 21 cm radio lines.

Methods. To investigate the properties of the 21 cm radio lines, the profiles of “The Leiden/Argentine/Bonn (LAB) Survey of Galactic H I” are decomposed into Gaussian components using a fully automatic algorithm. We focus on some regions with an increased number of Gaussians in phase space, defined by the component central velocity (V_C) and the full width at the level of half maximum (FWHM). To separate the Gaussians responsible for the phase-space density enhancements, we model the width distributions of Gaussian components at equally-populated velocity intervals, using lognormal distributions.

Results. We study the Gaussians, which parameters fall into the regions of the phase-space density enhancements at $(V_C, \text{FWHM}) \approx (-131^{+33}_{-43}, 27^{+9}_{-7})$, $(164^{+71}_{-49}, 26^{+9}_{-7})$ and $(-49^{+11}_{-14} \text{ km s}^{-1}, 23^{+10}_{-7} \text{ km s}^{-1})$, where the indexes indicate the half widths at the level of half maximum (HWHM) of the enhancements. The sky distribution of the Gaussians, corresponding to the first two concentrations, very well represents the sky distribution of HVCs, as obtained on the basis of the traditional definition of these objects. The Gaussians of the last concentration correspond to IVCs. Based on this identification, the division line between IVCs and HVCs can be drawn at about $|V_C| = 74 \text{ km s}^{-1}$, and IVCs can be identified down to velocities of about $|V_C| = 24 \text{ km s}^{-1}$. Traces of both IVCs and HVCs can also be seen in the sky distribution of Gaussians with $\text{FWHM} \approx 7.3 \text{ km s}^{-1}$. In HVCs, these cold cores have small angular dimensions and low observed brightness temperatures T_b . In IVCs, the cores are both larger and brighter.

Conclusions. When neglecting the general decrease in the amount of gas at higher $|V_{\text{LSR}}|$, the IVCs and HVCs are observed as distinctive maxima in the (V_C, FWHM) distribution of the Gaussians, representing the structure of the 21 cm radio lines of the Galactic H I. This definition is less dependant than the traditional one, on the differential rotation model of the Galaxy. The consideration of line-width information may enable IVCs and HVCs to be better distinguished from each other, and from the ordinary Galactic H I.

Key words. ISM: atoms – ISM: clouds – Radio lines: ISM

1. Introduction

In historical reviews, Wakker (2004) and Wakker et al (2004) state that early surveys of high-velocity H I clouds (HVCs), completed in the Netherlands, were concentrated at high Galactic latitudes, where normal disc gas has a low velocity. Velocities were reported relative to the Local Standard of Rest (LSR), using a limit of $|V_{\text{LSR}}| > 90$ or 100 km s^{-1} to define HVCs. During the course of these surveys, gas at velocities between -50 and -100 km s^{-1} was also found in many different directions. These objects were called intermediate-velocity clouds (IVCs). In this situation, a division of tasks was decided upon: astronomers of Leiden would analyse the high-velocity gas ($V_{\text{LSR}} < -80 \text{ km s}^{-1}$), while those at Groningen would concentrate on the IVCs.

As we can see, the velocity limits in these definitions are arbitrary, uncertain and partly based on historical arguments. A more physical approach to distinguishing of HVCs was introduced by Wakker (1991), who defined the “deviation velocity”, V_{DEV} , to be the difference between the LSR velocity of the cloud and the extreme velocity allowed by Galactic differential rotation in a particular direction. However, de Heij et al. (2002) presented

a slightly different definition of the deviation velocity, which allows for a Galactic Warp.

The definition of IVCs has remained uncertain. Albert & Danly (2004) state that IVCs are dynamically significant gas with velocities outside the range of the sum of Galactic rotation and Galactic velocity dispersion, but not as extreme as the velocities of HVCs. Numerically, they propose the velocity range $20 < |V_{\text{LSR}}| < 100 \text{ km s}^{-1}$, but velocities below 40 km s^{-1} can often be caused by differential Galactic rotation. Some authors have argued that the division between HVCs and IVCs, based on the LSR velocity, may be artificial. However, Wakker (2001) found that IVCs appear to exist approximately 1 kpc from the Galactic plane, while HVCs with known distance limits lie at $|z| > 3 \text{ kpc}$ (Wakker 2004).

The situation with HVCs and IVCs is further complicated by the fact that the gas with a velocity, which is dynamically unusual or significant in its local or Galactic frame, may appear close to 0 km s^{-1} with respect to the LSR. Therefore, it may be interesting to define these objects in way that is not based only on models of Galactic differential rotation. In this paper we try to identify both IVCs and HVCs using the frequency distribution of the Gaussian component parameters, derived in the decompo-

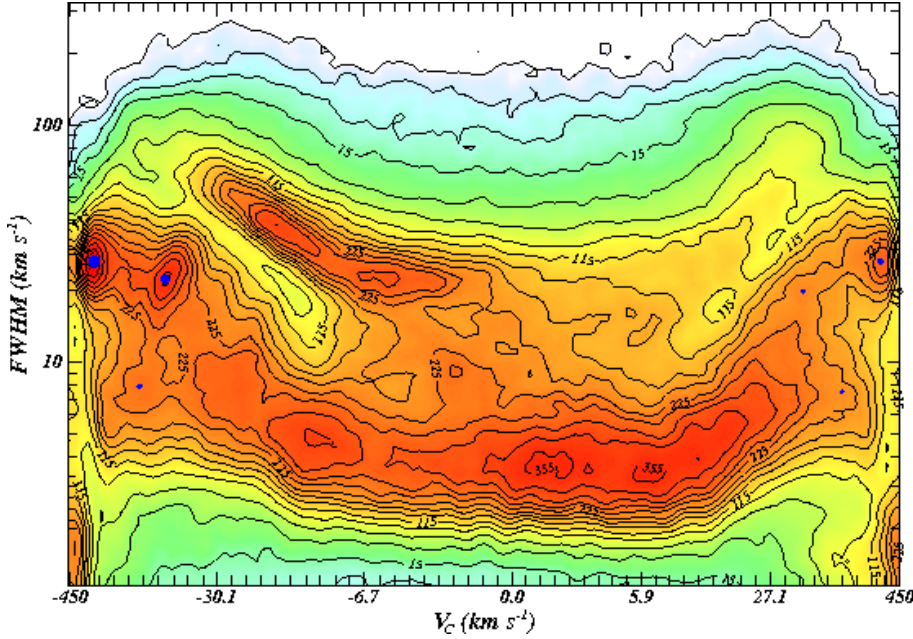


Fig. 1. Distribution of Gaussian parameters in the (V_C, FWHM) plane. The x-axis is linear for the queue numbers of the Gaussians in the ascending sequence of the component velocities. The corresponding velocity scale is stretched around $V_C = 0 \text{ km s}^{-1}$ and compressed at higher velocities. To illustrate this, the ticks on the x-axis are drawn at $-450, -184, -117, -94, -75, -63, -54, -47, -41, -35, -30.1, -25.6, -21.8, -18.5, -15.6, -13.3, -11.4, -9.9, -8.6, -7.6, -6.7, -5.8, -5.0, -4.3, -3.6, -3.00, -2.38, -1.78, -1.18, -0.57, 0.00, 0.56, 1.14, 1.71, 2.29, 2.89, 3.6, 4.3, 5.1, 5.9, 6.9, 7.9, 9.2, 10.7, 12.5, 14.9, 17.9, 21.9, 27.1, 34, 43, 54, 65, 79, 95, 121, 206$ and 450 km s^{-1} . The y-axis is logarithmic in FWHM. The contour lines are drawn at the levels of 1, 3, 7, 15, 35, 60, 90, 115, 145, 170, 195, 225, 250, 280, 315, 355, 395 and 445 Gaussians per counting bin. The frequency enhancements, discussed in the text, are marked with blue circles.

sition of the Leiden/Argentine/Bonn (LAB) full sky database of H I profiles (Kalberla et al 2005).

A detailed justification for the use of Gaussian decomposition, in such a study, was provided by Haud & Kalberla (2007, hereafter Paper III). The program that decomposes data from large 21 cm H I line surveys into Gaussian components, was described in the first paper of this series (Haud 2000, hereafter Paper I). The observational data for decomposition are from the LAB database of H I 21 cm line profiles, which combines the new revision (LDS2, Kalberla et al. 2005) of the Leiden/Dwingeloo Survey (LDS, Hartmann 1994), and a similar Southern sky survey (IARS, Bajaja et al. 2005) completed at the Instituto Argentino de Radioastronomía. The LAB database is described in detail by Kalberla et al (2005). Our method of Gaussian decomposition generated 1 064 808 Gaussians for 138 830 profiles from LDS2, and 444 573 Gaussians for 50 980 profiles from IARS.

In Paper II (Haud & Kalberla 2006), we analysed the distributions of the parameters of the obtained Gaussians. We focused mainly on the separation of the components describing different artefacts of the observations (interferences), reduction (baseline problems) and the decomposition (separation of signal from noise) process. In Paper III, we introduced the study of the width distributions of the Gaussian components at equally-populated velocity intervals, and demonstrated that for Gaussians with relatively small LSR velocities ($-9 \leq V_C \leq 4 \text{ km s}^{-1}$) it is possible to distinguish three or four groups of preferred line widths. The mean widths of these groups are $\text{FWHM} = 3.9 \pm 0.6, 11.8 \pm 0.5, 24.1 \pm 0.6$, and $42 \pm 5 \text{ km s}^{-1}$. In the present paper, we continue the analysis of the distribution of the Gaussian parameters, but focus on the components with the central LSR velocities $|V_C| \geq 10 \text{ km s}^{-1}$. We demonstrate that some frequency enhancements in this region define two classes of objects whose general properties are similar to those of the IVCs and HVCs, defined by more traditional velocity criteria.

2. The velocity – width distribution of the Gaussians

In Paper III, we introduced the diagram (Fig. 2. of Paper III) of the frequency distributions of Gaussian component widths at

equally-populated velocity intervals. We define the Gaussians by the standard formula

$$T_b = T_{b0} e^{-\frac{(V-V_C)^2}{2\sigma_V^2}}, \quad (1)$$

where T_b is the brightness temperature, and V is the velocity of the gas relative to the Local Standard of Rest. $T_{b0} > 0$ is the height of the Gaussian at its central velocity V_C . We characterise the widths of the components by their full width at the level of half maximum (FWHM), which is related to the velocity dispersion σ_V , obtained from our decomposition program, by a simple scaling relation $\text{FWHM} = \sqrt{8 \ln 2} \sigma_V$.

Because the Gaussian functions fitted to the complex H I profiles, close to the Galactic plane, cannot be directly interpreted in terms of the properties of gas clouds, in Paper III we focused on the higher Galactic latitudes, and stressed the differences in the (V_C, FWHM) frequency distribution of Gaussians at different latitudes. In this paper, we concentrate on higher velocities, where differences in the distributions for different latitude ranges are smaller, and therefore present, in Fig. 1, the distribution of Gaussians for all Galactic latitudes. To construct this figure, we arranged all Gaussians with central velocities in the decomposition range ($-460 < V_C < 396 \text{ km s}^{-1}$ in the LDS2 and $-437 < V_C < 451 \text{ km s}^{-1}$ in the IARS; for details see Papers I and II), in ascending order of their V_C . We then grouped the sequence into 129 bins of an equal number of Gaussians, rejecting some Gaussians with the most extreme velocities. We binned the line widths in equal steps of $\lg(\sigma_V)$ of 0.025. The isolines in Fig. 1 provide the number of Gaussians at each of such two-dimensional parameter interval.

In Fig. 1, the region most densely populated by Gaussians, lies in the lower part of the figure at relatively small LSR velocities. In Paper III, we demonstrated that most of these Gaussians represent the cold neutral medium of the Galactic disc. In the present figure, this low-velocity region is also seriously contaminated by Gaussians from the strongest H I profiles, close to the Galactic plane, parameters of which are not directly related to the properties of the real gas. At somewhat higher negative velocities (from $V_C \approx -2$ to -40 km s^{-1}) and larger line widths (from $\text{FWHM} \approx 20$ to 70 km s^{-1}), we can see an elongated region of high Gaussian density. We

will not discuss this feature in the present paper. At even higher negative velocities in Fig. 1, we can see two high-density regions centred at $(V_C, \text{FWHM}) \approx (-131^{+33}_{-43}, 27^{+9}_{-7})$ and $(-49^{+11}_{-14} \text{ km s}^{-1}, 23^{+10}_{-7} \text{ km s}^{-1})$ (the largest blue circles in Fig. 1). Here the indexes of the values of the velocities and line widths provide estimates of the half widths of the corresponding distributions at the level of half maximum. At positive velocities, only one such frequency enhancement is clearly visible about $(V_C, \text{FWHM}) \approx (164^{+71}_{-49} \text{ km s}^{-1}, 26^{+9}_{-7} \text{ km s}^{-1})$. These enhancements contain the Gaussians of our main interest in the present paper. At even higher negative and positive velocities, two concentrations of narrow Gaussians are clearly visible (at the bottom corners of the figure). These are generated by the presence of spurious Gaussians, as discussed in Paper II.

In Paper III, we demonstrated that, for Gaussians with relatively small LSR velocities, it is possible to distinguish three or four groups of preferred line widths. Similar line-width groups appear to exist at higher velocities, but their mean widths depend on the velocity of the selected Gaussians, and only in relatively small velocity intervals, we can consider the line-width distributions to be nearly independent of the central velocity of the Gaussians. Therefore, we must require a separate model of the width distribution, for each equally-populated velocity interval. Only this would make it possible to distinguish between components, belonging to different line-width groups.

As in the case of lower velocities, we model all the width distributions with a sum of lognormal functions defined by

$$f_{\mu, \sigma^2}(x) = \begin{cases} 0 & (x \leq 0) \\ \frac{f_0}{\sqrt{2\pi\sigma^2 x}} e^{-\frac{(\ln(x)-\mu)^2}{2\sigma^2}} & (x > 0), \end{cases} \quad (2)$$

where f_0 , μ and σ may be considered as free parameters for fitting the model distribution to the observed one. As in Paper III, we used, in most cases, four lognormal functions for each modelled velocity interval. Only at the highest positive and negative velocities, we introduced an additional lognormal to reject the spurious Gaussians, causing the enhancements at the lower corners of Fig. 1.

Many different density functions are available that can model the distributions of Gaussian widths, which are defined to be positive. We chose to use the lognormal function because its usage is technically convenient: if a parameter is distributed according to the lognormal law, the distribution of the logarithms of the parameter is described by a Gaussian. Mebold (1972) also argued that his narrow and shallow components could be identified most easily, when the line-width distribution is studied in a logarithmic scale. Moreover, from all tested density functions, the lognormal provided the best fits.

The described modelling was relatively easy for the negative velocity part of the distribution in Fig. 1, but more ambiguous for positive velocities, as there the number of Gaussians is smaller, equally-populated velocity intervals are wider, and the density maxima are less obvious. At the same time, it can be seen from Fig. 1 that the general structure of the distribution is similar for negative and positive velocities. The enhancements are weaker at positive velocities, but we may find that these weaker maxima are at approximately the same positions as for negative velocities: a strong enhancement at $(V_C, \text{FWHM}) \approx (-131 \text{ km s}^{-1}, 27 \text{ km s}^{-1})$ corresponds to a weaker one at $(164 \text{ km s}^{-1}, 26 \text{ km s}^{-1})$, and a weaker enhancement at $(-49 \text{ km s}^{-1}, 23 \text{ km s}^{-1})$ corresponds to an even weaker one at about $(44 \text{ km s}^{-1}, 20 \text{ km s}^{-1})$. Therefore, to consider the positive velocity information, we decided to average the positive and negative velocity sides of the distribution (Fig. 2a), and to

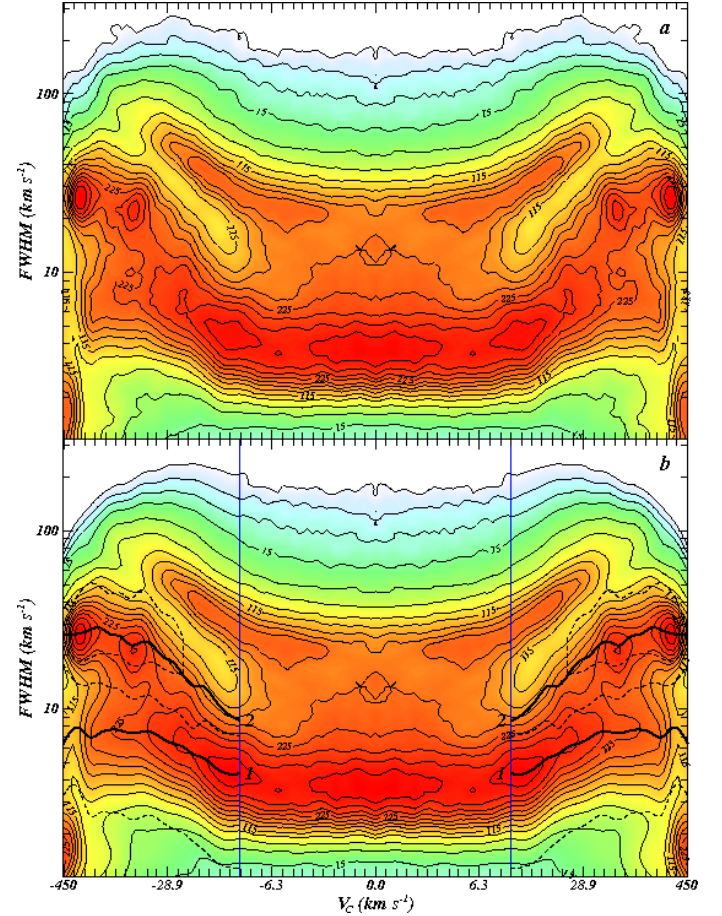


Fig. 2. Symmetrised distribution of Gaussian parameters in the (V_C, FWHM) plane (a) and the corresponding model distribution (b). The contour lines are obtained in the same way as in Fig. 1. The ticks on the x-axis are drawn at 0.00, ± 0.54 , ± 1.10 , ± 1.66 , ± 2.22 , ± 2.79 , ± 3.4 , ± 4.1 , ± 4.7 , ± 5.5 , ± 6.3 , ± 7.2 , ± 8.2 , ± 9.3 , ± 10.8 , ± 12.4 , ± 14.5 , ± 17.1 , ± 20.3 , ± 24.2 , ± 28.9 , ± 35 , ± 41 , ± 49 , ± 57 , ± 67 , ± 80 , ± 98 , ± 122 , ± 203 and $\pm 450 \text{ km s}^{-1}$. The vertical blue lines indicate the range of modelling ($|V_C| \geq 9.38 \text{ km s}^{-1}$), the thick black lines mark the run of the peaks of the two line-width groups and the dashed lines on both sides of the thick lines give the extent of the regions, where the Gaussians belong respectively to group 1 or 2 with the probability higher than 75%.

construct the same model for the positive and negative velocities (Fig. 2b).

During the modelling, we encountered one additional problem. When the values of f_0 and μ for lognormal distributions were well determined, the values of σ of different lognormal functions were often strongly correlated with each other. This occasionally meant that the σ of the same line-width component, had very different values for neighbouring velocity intervals. Numerically, when the mean uncertainties in fitting f_0 and μ were 8.6% and 2.5%, respectively, the corresponding uncertainty in the values of σ was about 38%. To overcome this problem, we first fitted all width distributions, considering f_0 , μ and σ of all lognormal functions as free parameters. We then analysed the σ of each line-width component, as a function of the number of the velocity interval, and applied natural smoothing splines. In the second run of fitting of the sums of lognormal functions to the width distributions of Gaussians in different equally-populated

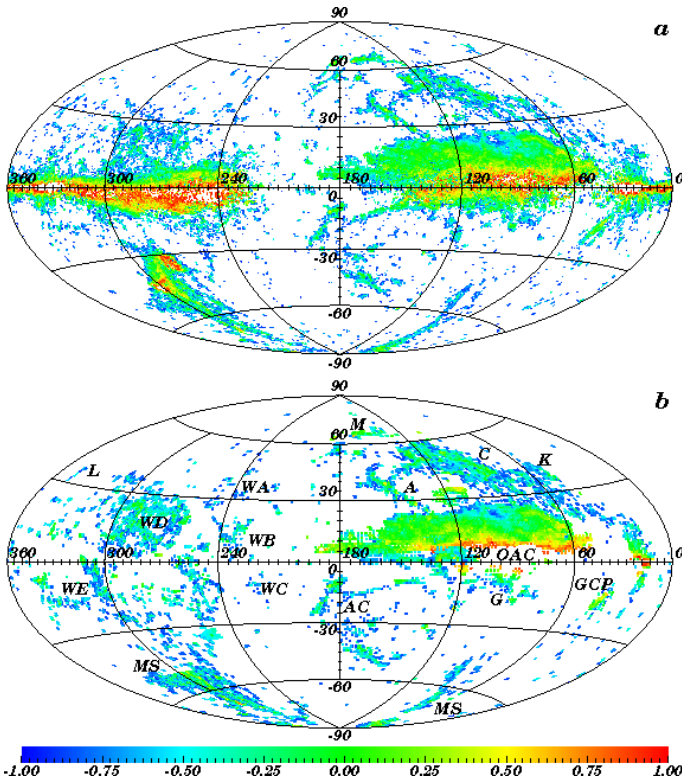


Fig. 3. Sky distribution in Galactic coordinates of the Gaussians, belonging to the second line-width group at velocities $|V_C| > 74 \text{ km s}^{-1}$ (a) and the brightness of the high-velocity hydrogen clouds from the Hulsbosch & Wakker (1988) and Morras et al. (2000) surveys (b). The labels with capital letters indicate the larger HVC complexes according to Wakker (2004). In the upper panel the colours encode the values of $\lg(T_p)$. In the lower panel the same colour scale corresponds to the logarithms of the brightness temperatures of the HVC detections. In both panels near the Galactic plane the strongest Gaussians with T_p or $T_{b0} > 10 \text{ K}$ are not plotted.

velocity intervals, we replaced the values of σ , obtained in the first fitting, with the results of the smoothing, and kept the values of σ fixed while iterating f_0 and μ . The resulting model distribution is provided in Fig. 2b. We are not interested in velocities close to zero, which were discussed in Paper III. The modelling was performed only for $|V_C| \geq 9.38 \text{ km s}^{-1}$, indicated in Fig. 2b with blue vertical lines.

After defining line-width groups of Gaussians using different lognormal functions, it is interesting to find out how these groups are related to actual gas within and about the Galaxy. To study this question, we need to determine which Gaussian belongs to which line-width group. The frequency distributions of Gaussians of different groups, however, overlap considerably and we are unable to identify with full confidence the Gaussians belonging to any particular group. However, using our model distribution, we can estimate for every Gaussian the probability of belonging to some particular line-width group.

So, let us define the probability that a Gaussian belongs to the line-width group i as

$$p_i = \frac{f_i(V_C, \sigma_V)}{\sum_{j=1}^n f_j(V_C, \sigma_V)}, \quad (3)$$

where f_i is the density function of the lognormal distribution, as defined by Eq. 2, corresponding to the i -th line-width group,

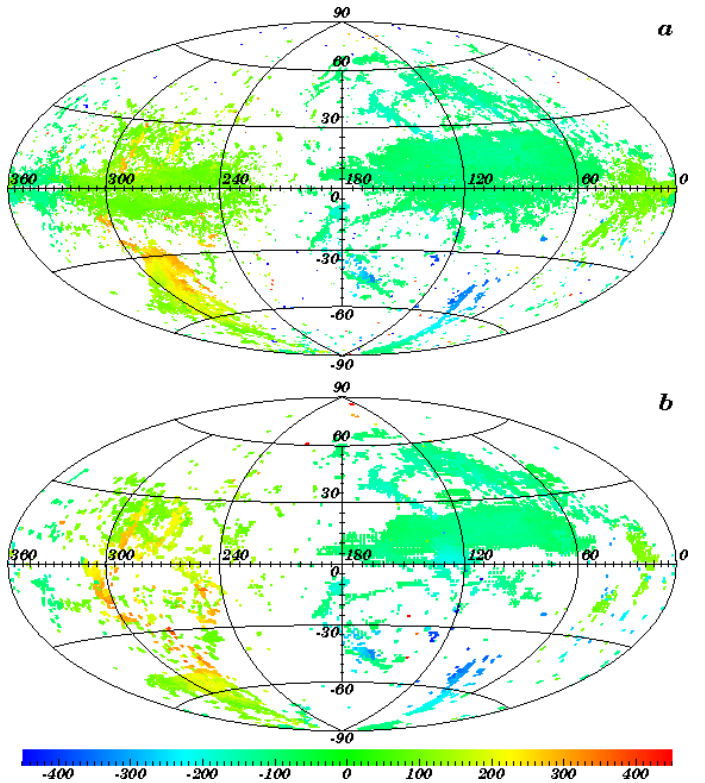


Fig. 4. Same as Fig. 3, but the colours represent the LSR velocities of the gas.

V_C is the central velocity, and σ_V the width of the particular Gaussian and $n = 4$ or 5 , depending on the velocity interval under consideration. To study the sky distribution of the Gaussians from the selected line-width group i , we can then plot $T_p = T_{b,0} p_i$, the heights of Gaussians $T_{b,0}$, multiplied by the probability that the Gaussian belongs to this line-width group p_i . In this way, all the Gaussians from our decomposition will be presented on each plot. However, the brightness of the Gaussians, for which the probability of belonging to a particular line-width group is low, is suppressed considerably by these small probabilities. To enhance the contrast in plots even more, and because the noise level of the LAB Survey is about $\langle \sigma_{\text{rms}} \rangle = 0.09 \text{ K}$ (see Paper II), we also do not plot Gaussians for which $T_p < 0.1 \text{ K}$. In this way we exclude, from the sky plots, most of the weak Gaussians, which represent the survey baseline problems. Stronger spurious Gaussians are excluded, according to the criteria described in Paper II.

3. High velocities

As stated in the previous section, we are mostly interested in frequency enhancements in Fig. 1, which are centred at $(V_C, \text{FWHM}) \approx (-131, 27)$, $(-49, 23)$, $(44, 20)$ and $(164 \text{ km s}^{-1}, 26 \text{ km s}^{-1})$. In our model, these enhancements correspond to the line-width group 2 as labelled in Fig. 2b. As can be seen from Fig. 1, at negative velocities this line-width group clearly forms two frequency enhancements in different velocity regions. These frequency enhancements are separated by the region, more dominated by Gaussians of other line-width groups, and the second group has a frequency minimum at about $|V_C| = 74^{+7}_{-6} \text{ km s}^{-1}$. The same appears to be true for positive velocities, but there the picture is considerably less clear.

We concentrate first on Gaussians of the second line-width group with $|V_C| > 74 \text{ km s}^{-1}$. Fig. 3a illustrates the sky distribution of brightness temperatures of these components, and Fig. 4a provides the distribution of LSR velocities for the same Gaussians. In Fig. 3b, we present the sky distribution of brightness temperatures of HVCs with $T_b > 0.1 \text{ K}$ as compiled from Hulsbosch & Wakker (1988) and Morras et al. (2000) catalogues, and Fig. 4b provides their velocity distribution. Comparing the panels of these figures, a surprising similarity is visible between the distributions for the objects, selected from different observational data by different procedures.

The HVC catalogues by Hulsbosch & Wakker (1988) and Morras et al. (2000) are based on H I profiles with a velocity resolution of about 16 km s^{-1} and a noise level of about $\langle \sigma_{\text{rms}} \rangle = 0.015 \text{ K}$. All the observed profiles were scanned visually for the presence of components at high velocities, using two selection criteria: the component should have a brightness temperature $T_b \geq 0.05 - 0.08 \text{ K}$ and should have $|V_{\text{LSR}}| \geq 100 \text{ km s}^{-1}$ or 80 km s^{-1} . Figs. 3a and 4a are based on the LAB Survey, which has a velocity resolution of about 1 km s^{-1} , and a noise level of about 0.09 K . Both figures were made without any visual inspection of the profiles, using statistical data for Gaussians (mostly $T_b \geq 0.13 \text{ K}$) obtained in a fully automatic decomposition of the survey profiles. In our study the first selection criterion was the line width, which was not directly used by Hulsbosch & Wakker (1988) and Morras et al. (2000). Nevertheless, all well-known HVC complexes are clearly visible in both figures.

Besides the differences, described above, there is a selection criterion almost in common for panels a and b of Figs. 3 and 4 – the velocity range. For panels a of these figures, we have used Gaussians with $|V_C| > 74 \text{ km s}^{-1}$. Figs. 3b and 4b represent the gas with $|V_{\text{LSR}}| \geq 100 \text{ km s}^{-1}$ or 80 km s^{-1} . It is possible that the similarity of these velocity limits is the main factor that determines the similarity of the sky distributions. However, in this case, Figs. 3a and 4a must remain unchanged if we keep the velocity limits, defined above, but instead of Gaussians from line-width group 2, use those from some other group (number 1, for example). The actual results do not confirm this expectation. The sky distribution of the Gaussians of the first line-width group (Fig. 5a) is different from that of the second line-width group (Fig. 3a). The well-populated HVC complexes are no longer visible. In Fig. 5a, only small concentrations of weak dots are observed in the regions, which in Fig. 3a are populated by the largest HVC complexes.

This result becomes understandable in the light of the discussion by Kalberla & Haud (2006): most of the high-velocity clouds have a well-defined two-component structure, where the cold HVC phase has a typical line-width of about 7.3 km s^{-1} , and exists only within more extended broad-line regions, typically with $\text{FWHM} \approx 27.2 \text{ km s}^{-1}$. Therefore, we may state that the modelling of the line-width distribution of Gaussians permits us to separate the warm and cold gas phases in HVCs, as it was also possible for the local H I gas. However, for the local gas the corresponding line widths were $\text{FWHM} = 3.9$ and 24.1 km s^{-1} .

There are still Gaussians belonging neither to line-width component 1 nor to component 2. Their sky distribution is given in Fig. 5b. This figure shares the same velocity limit as Figs. 3a and 5a, but here we can see only rather weak traces of all HVC structures. Of course, it would be nice, if in this figure there were no traces of HVCs at all, but we must remember that the separation of the Gaussians into different line-width groups is only statistical and the probabilities are determined from the smoothed model. It seems that this model has worked most badly for some parts of the Magellanic Stream.

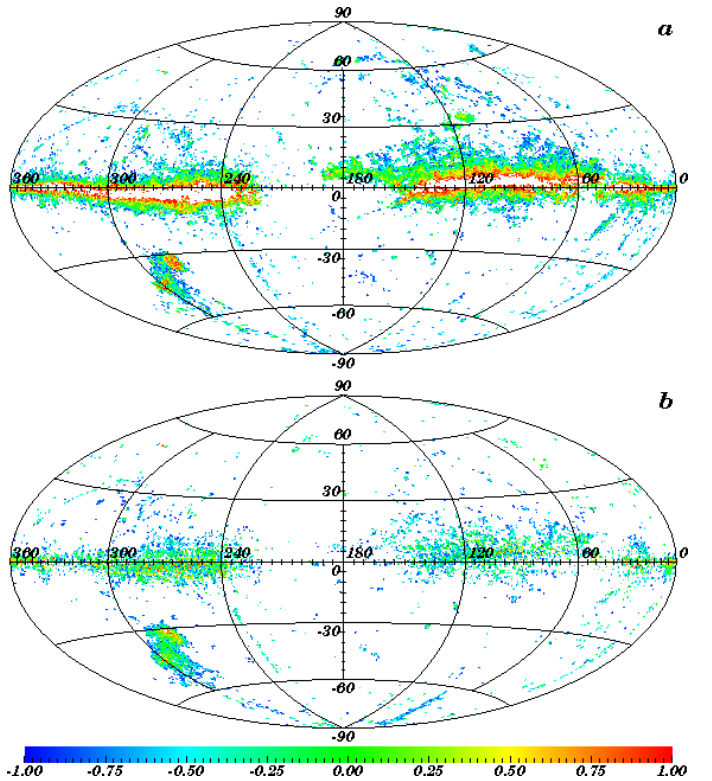


Fig. 5. Same as Fig. 3a, but for the line-width group 1 (a) and for all Gaussians, except those belonging to the line-width groups 1 and 2 (b).

Besides the similarities between Figs. 3a and 3b, there are also considerable differences. The most obvious one is the presence in Fig. 3a of a large number of strong Gaussians, close to the Galactic plane and in the region of the Magellanic Clouds. However, close to the Galactic plane the Gaussians are obtained from the decomposition of very complex H I profiles of the Galactic disc, in which the real gas structures are heavily blended with each other; these Gaussians should therefore not be considered as directly representing the properties of the ISM. The same regions are heavily populated in both panels of Fig. 5. In these regions, the decomposition provides the Gaussians of all possible parameters, and without any concentration of these parameter values in any region of parameter space. In Fig. 1, these Gaussians form the general background against which we may distinguish the features, more directly representing the properties of Galactic H I. The same holds also for the main bodies of the Magellanic Clouds.

As we can estimate from the comparison of different sky distribution figures, close to the Galactic plane, the region of “confusion” lies generally at $|b| < 15^\circ$. Above this latitude limit, the distribution of Gaussians appears to be representative of the properties of HVCs. This is of particular importance for the Outer Arm Cloud (OAC). In early studies (Habing 1966, Hulsbosch & Wakker 1988), this complex was considered to be an HVC. Verschuur (1975) and Haud (1992) have modelled the complex as part of the outer disc of the Milky Way. Based on the deviation velocity, a recent review (Wakker 2004) considers the OAC to be an intermediate-velocity cloud. From a statistical analysis of the Gaussian parameters, we are unable to conclude much about the OAC close to the Galactic plane. In the parts most distant from the galactic plane however, the gas properties appear to agree with the gas properties in HVCs.

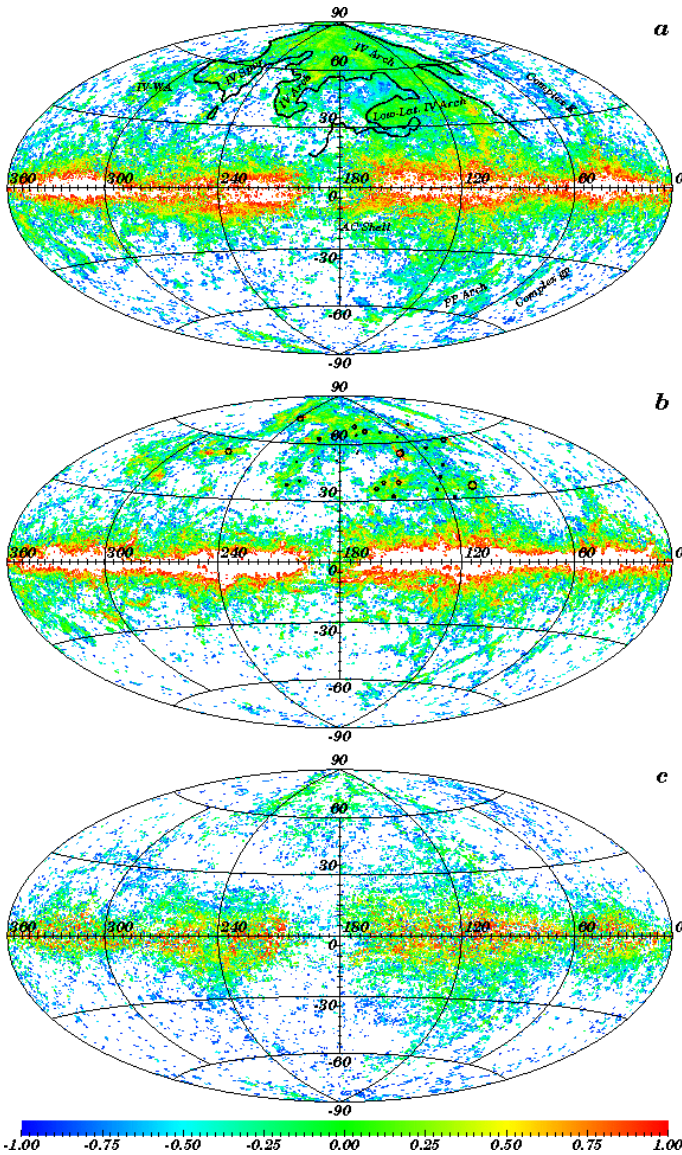


Fig. 6. Same as Fig. 3a, 5a and 5b, but for the velocity interval $24 < |V_c| < 74 \text{ km s}^{-1}$. (a) The sky distribution of the Gaussians, belonging to the second line-width group. The solid contour and the labels indicate the region of major intermediate-velocity gas features according to Kuntz & Danly (1996) and Wakker (2001). (b) The sky distribution of the Gaussians belonging to the first line-width group. The circles indicate the locations of the intermediate-velocity gas clumps from the catalogue by Kuntz & Danly (1996). (c) The sky distribution of all Gaussians, except the ones corresponding to the first and second line-width group.

In conclusion, we note that two different approaches to identifying high-velocity H I gas at high Galactic latitudes ($|b| > 15^\circ$), have produced remarkably similar results. We cannot, of course, consider these methods to be completely independent ones. The classical definition of HVCs is fully based on their LSR velocities, and the model of differential rotation of the Galactic disc. The horizontal structure of Fig. 1 is largely determined by the Galactic differential rotation as well, but a comparison of Figs. 3a, 5a and 5b demonstrates that velocity is not the only factor that defines HVCs. Moreover, when using the statistical distribution of Gaussian parameters, we can es-

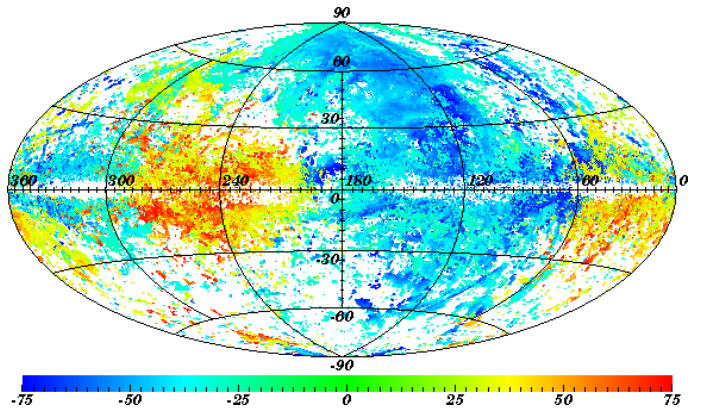


Fig. 7. Same as Fig. 6a, but the colours represent the LSR velocities of the gas.

timate the extent of the velocity and line-width intervals populated by the components, which most likely represent HVCs. Unfortunately, the analysis becomes complicated and unreliable, when approaching the Galactic plane, where the classic definition of HVCs also has the greatest trouble.

4. Intermediate velocities

We have so far considered line-width groups only for velocities $|V_c| > 74 \text{ km s}^{-1}$. There is however, another maximum at lower velocities, which peaks at $V_c \approx -49 \text{ km s}^{-1}$. The lower velocity limit of this frequency enhancement is questionable. The concentration about $(V_c, \text{FWHM}) \approx (-49 \text{ km s}^{-1}, 23 \text{ km s}^{-1})$, in Fig. 1, reaches its HWHM at $V_c \approx -38 \text{ km s}^{-1}$. The relative frequency of group-2 Gaussians drops to the level of the minimum between two peaks in Fig. 2b at about $|V_c| = 35 \text{ km s}^{-1}$, but even after this, group 2 can still modelled until about $|V_c| = 24 \text{ km s}^{-1}$. At even lower velocities, the determined parameters of the second line-width group became rather uncertain, the corresponding Gaussians are relatively few in number, and we do not discuss these velocities.

The sky distribution of the Gaussians of the second line-width group in the intermediate velocity range $24 < |V_c| < 74 \text{ km s}^{-1}$ is shown in Fig. 6a. Their velocity distribution is provided in Fig. 7. In Fig. 6a, we mark with a thick solid line, the $1.8 \times 10^{19} \text{ cm}^{-2}$ surface density contour of the intermediate-velocity hydrogen clouds, as published in Fig. 8 of Kuntz & Danly (1996). Some additional IVC complexes, identified by Wakker (2001), are also labelled. We see that, as in the case of HVCs at higher velocities, in the intermediate velocity range the distribution of Gaussians, from the second line-width group, closely follows the main features of the distribution of the IVCs. This indicates that both HVCs and IVCs appear to represent related features in different velocity ranges.

As for HVCs, in the intermediate velocity range, many Gaussians of the first line-width group are concentrated in sky regions populated by IVC gas, of the second line-width group (Fig. 6b). Among these are Gaussians, for which the probabilities of belonging to the first or second line-width group are nearly equal to each other. These Gaussians are plotted both in Figs. 6a and 6b. A more detailed examination of the situation however, indicates that this is not the only effect. In many sky positions in the region covered by IV Arches and Spur, the decomposed hydrogen profiles contain Gaussians from both line-width groups. Altogether the profiles for 36 375 sky positions at $|b| \geq 30^\circ$ contain Gaussians, which can be classified with at least

50% confidence to belong to the first or second line-width group, and of these sky positions, 9 015 profiles, or nearly 25%, contain both the Gaussians of the first and the second line-width group.

The comparison of Figs. 6a and 6b reveals differences in the properties of the IVC components, corresponding to the two different line-width groups. When the clouds corresponding to the first line-width group appear to be brighter and clumpier, those corresponding to the second line-width group cover the sky in the regions of IV Arches and Spur more uniformly, but with smaller average brightness. A similar behaviour by the intermediate-velocity gas was noted by Kuntz & Danly (1996), who stated that the bulk of the intermediate-velocity gas is primarily composed of clumps, which appear to be surrounded by a lower column density envelope.

In their Table 1, Kuntz & Danly (1996) published the catalogue of denser clumps, which we have presented in Fig. 6b as circles centred at the positions of the peak column densities of the clumps. Unfortunately, the above-mentioned Table 1 does not contain much information about the shapes and sizes of the clumps. We therefore plot these objects in Fig. 6b, as circles of radii proportional to the clump peak intensities, which are provided by Kuntz & Danly (1996). As can be seen, the brighter clumps from the catalogue coincide with the concentrations of Gaussians in our figure. The correspondence is more problematic for the weakest clumps (for which the circles have been reduced in size to dots), but here we must consider that the paper by Kuntz & Danly (1996) was based on the Bell Laboratories H I survey described by Stark et al., (1992). The rms noise per channel for this survey was 0.017 K, a value more than 5 times lower than for LDS, such that many of the weakest clumps detected in these data may not be detected by us. Moreover, the sampling grid of the Bell Laboratories survey was 2° in declination and about 0.5 in right ascension, which was rebinned by Kuntz & Danly (1996) into a regular grid, comparable to the beam size of about 2.5 , of the horn reflector used. As a result, the locations of the circles in Fig. 6b should not be considered to be accurate.

Our results appear to confirm that the IVCs have a two-component structure: brighter clumps, whose emission lines correspond to the first line-width group; and lower column density envelopes, whose emission can be described by Gaussians of the second line-width group. A similar two-component structure is found for HVCs, for which the velocity profiles are often composed of a broad (FWHM $\sim 20 - 25 \text{ km s}^{-1}$), and a narrow ($\sim 8 \text{ km s}^{-1}$) component (Wakker & Woerden 1997; mean FWHM $\approx 27.2 \text{ km s}^{-1}$ and 7.3 km s^{-1} according to Kalberla & Haud 2006). The corresponding mean line widths for IVCs, are FWHM $\approx 22.2 \text{ km s}^{-1}$ and 7.2 km s^{-1} , respectively.

Fig. 6c corresponds to Fig. 5b for the high velocity region and demonstrates that in the sky distribution of the Gaussians, not belonging to line-width groups 1 or 2, we can see only weak traces of the IVCs. These traces once again, are mostly caused by difficult-to-classify, relatively bright Gaussians, which appear both in Figs. 6a or 6b and Fig. 6c. Moreover, the visibility of these traces is enhanced in Fig. 6c, because we do not plot in any sky distribution, the Gaussians, which are considered to be spurious, according to the selection criteria described in Paper II. By adding these components, Fig. 6c would be more homogeneously filled with random dots. Only the Galactic plane would remain visible, as a region of slightly enhanced concentration of the Gaussians. Close to the Galactic plane, however, the Gaussian decomposition itself is badly determined, and Gaussians of all possible parameters are found. This region is therefore, filled by dots in all sky distribution figures.

Finally, according to our knowledge, so far there have not been any systematic searches of IVCs in the southern sky (the blank region in Fig. 3 of Wakker 2004). As LAB includes both the northern and the southern data, our Fig. 6 also contains information on the southern IVCs. However, as we can see, in this figure the regions, observable only from the southern hemisphere of the Earth, are almost empty, and the only possible new IVC complexes are the concentrations of dots in the region $280^\circ < l < 300^\circ$, $-35^\circ < b < -15^\circ$. In this region, we can see 2-3 “clouds” with typical IVCs properties: relatively small and bright concentrations of the group-1 Gaussians, surrounded by wider envelopes of the weaker group-2 Gaussians.

5. Discussion

We have demonstrated that both the HVCs and IVCs could be identified as concentrations of Gaussians in (V_C , FWHM) frequency plots. For both cloud types, we have identified a two-phase structure, where the cold phase, corresponding in Gaussian width distribution to group 1, exists within more extended broad-line (line-width group 2) regions. In this respect, both HVCs and IVCs appear to represent related dynamical features, in different velocity ranges. However, besides similarities, there are differences between the cloud types. The first difference can be seen in Fig. 1: at both negative and positive velocities the concentrations of Gaussians, corresponding to the envelopes of the IVCs, are located at lower line-widths than those corresponding to HVCs.

We have noted differences in the relative intensities of the cores and envelopes of HVCs and IVCs. In HVCs, the components obtained from LAB, and corresponding to the cold cores, are relatively weak, and the angular dimensions of the cores found are relatively small. The cores in IVCs appear to be larger, with more intense radiation. This could imply that both the linear dimensions and gas content, of the cores of HVCs and IVCs, are similar, but IVCs are closer to us, on average, than the HVCs. The cores of the more distant HVCs would then have smaller angular sizes, and fill the aperture of a 25 m telescope to a lesser extent than the more nearby cores of IVCs. As a result, they are detected more weakly. This interpretation is supported by Schwarz & Wakker (2004), who state that intermediate ($10'$) resolution observations of HVCs imply smaller core angular dimensions, and higher core brightnesses than measured at lower resolution. The explanation is also in agreement with distance estimates of HVCs and IVCs (Wakker 2004).

These differences in the apparent importance of the cold cores in HVCs and IVCs, may help to distinguish between HVCs and IVCs. For example, Fig. 6 illustrates the sky distribution of Gaussians with intermediate velocities. In Fig. 6a, we observe a concentration of points at $l \approx 300^\circ$, $-90^\circ < b < -65^\circ$. In Fig. 6b, we only see small concentrations of weak Gaussians in this region. This is typical of HVCs, and we know that the discussed concentration of relatively low velocity is a part of the Magellanic Stream. In general, the velocities in the Magellanic Stream are high, but Fig. 6 presents only a small part of the full stream. In this part the velocity is relatively low, due to projection effects.

A more interesting example is found in Figs. 3a and 5a. In Fig. 3a (line-width group 2), we find two weak concentrations of dots at $(l, b) = (120^\circ, 29^\circ)$ and $(110^\circ, 34^\circ)$. In Fig. 5a (line-width group 1), these clouds are considerably brighter, which is a characteristic of IVCs. The mean LSR velocities of the objects are -80.9 and -78.2 km s^{-1} , respectively. These velocities are slightly above the limit $|V_C| = 74 \text{ km s}^{-1}$, which we use to sepa-

rate IVCs from HVCs. There is usually, however, no sharp separation between statistical distributions. The velocity distributions of HVCs and IVCs probably partially overlap, as do the line-width distributions of Gaussians from the first and second line-width groups. Based on their core-envelope structure, we expect that the two clouds are, in fact, intermediate-velocity clouds with velocities that are characteristic of HVCs. The same is possibly true for the cloud around $(l, b, V_C) = (39^\circ, 63.5^\circ, -80.4 \text{ km s}^{-1})$, in Figs. 3a and 5a. The Magellanic Stream, however, is classified as an HVC, even though, in one part its velocities are more characteristic of IVCs.

In this context, it is interesting to consider the Outer Arm Cloud. From the comparison of our sky distribution images, it appears in most parts that the properties of the gas in the OAC correspond to those of the HVC. In two regions only, this large HVC complex could be overlaid with a considerable amount of IVC gas. One of these regions is located at about $l = 100^\circ$, and the corresponding IVC gas appears to form an extension of the high latitude IV Arch, to close to zero latitude. Another region with a large number of intermediate-velocity cores, located at $(l, b) = (179^\circ, 15^\circ)$, may for example be the northern extension of the AC Shell. In any case, the gas properties of the OAC appear to be different from those of normal gas in the Galactic disc.

Kalberla & Haud (2006) found that the cold cores of HVC complexes have a random velocity distribution, with a typical dispersion of 20 km s^{-1} . Kuntz & Danly (1996) found evidence that the infall velocity of IVCs reaches a maximum at positions of highest column density. Similar results can be seen in our Fig. 1: at negative velocities the line-width group-1 Gaussians, in the intermediate velocity range, reach a maximum in their frequency distribution at $(V_C, \text{FWHM}) = (-63.5 \text{ km s}^{-1}, 7.9 \text{ km s}^{-1})$, whereas the components of line-width group 2 have a corresponding maximum at $(V_C, \text{FWHM}) = (-49.4 \text{ km s}^{-1}, 22.4 \text{ km s}^{-1})$, i.e., the cold cores often have larger infall velocities than their warmer envelopes.

In Fig. 1, the distribution of group-1 Gaussians is contaminated by spurious components from profiles close to the Galactic plane. To consider this further, we made similar figures for the regions $|b| > b_{\text{lim}}$, with different $b_{\text{lim}} \geq 15^\circ$. In these figures, the frequency maximum of group-1 Gaussians, in the intermediate velocity range, is shifted to lower velocities, in most cases close to $V_C = -54 \text{ km s}^{-1}$. The location of the frequency maxima of group-2 Gaussians remains practically unchanged. This indicates that the velocity differences are only partly explained by the contamination.

At positive velocities, it is difficult to draw a similar conclusion. From symmetry considerations however, it is interesting to mention that there is a weak density enhancement at $(V_C, \text{FWHM}) = (74.9 \text{ km s}^{-1}, 7.5 \text{ km s}^{-1})$, but for higher values of b_{lim} , it disappears completely from the plots. At the same time, the density enhancement, corresponding to the envelopes of the positive velocity IVCs, becomes much more prominent in higher latitude plots, than in Fig. 1.

6. Conclusions

Different and almost arbitrary definitions of the IVCs and HVCs exist so far, and the main HVC catalogues (Hulsbosch & Wakker 1988, Morras et al. 2000) have been compiled by visual inspection of the observed profiles for the presence of components at high velocities. In this paper, we have tried an automated approach by decomposing all profiles into Gaussian components and studying the frequency distributions of the parameters of the obtained Gaussians. Our approach identifies most well-known

HVC and IVC complexes on the basis of remarkable density enhancements in particular regions of the $(V_C - \text{FWHM})$ frequency diagram of the Gaussian parameters. The general properties of objects, separated in this way are almost identical to the properties of IVCs and HVCs, defined in the traditional way:

- the sky distributions of T_b and V_{LSR} of statistically-identified IVCs and HVCs, are similar to those of the classical complexes;
- the division line between HVCs and IVCs most likely lies at about $|V_{\text{LSR}}| = 74 \text{ km s}^{-1}$;
- both HVCs and IVCs have a two-component core-envelope structure;
 - the cold cores of HVCs and IVCs have almost the same mean line-widths: $\text{FWHM} \approx 7.3$ and 7.2 km s^{-1} , respectively;
 - when the mean line-width of the envelopes of HVCs is $\text{FWHM} \approx 27.2 \text{ km s}^{-1}$, the corresponding value for IVCs is only 22.2 km s^{-1} ;
 - the angular dimensions and the brightnesses of HVC cores, derived using the LAB, are smaller than the corresponding values for the cores of IVCs.
- the infall velocities of the cores of IVCs often appear to be higher than the infall velocities of the corresponding envelopes.

The differences in the core-envelope structure of the HVCs and IVCs can provide additional information to help distinguish between the two cloud types.

Considering the frequency distribution, presented in Fig. 1, and other properties of IVCs and HVCs discussed in this paper, the suggestion by Kuntz & Danly (1996, see also Kerp et al. 1996, 1996) that IVCs were once HVCs that have decelerated on approach to the disc, appears plausible. In Fig. 1, a deep minimum is present between maxima, which correspond to negative-velocity IVCs and HVCs. This minimum could indicate that most observable intermediate-velocity clouds are the results of a large accretion event, or that the lifetime of IVCs and HVCs, is much longer than the interaction phase (deceleration time) between high-velocity clouds and the Galactic disc, or halo gas.

At the same time, it is commonly believed that the metallicities of HVCs are lower than those of IVCs (Wakker 2001), which makes the possibility of a relationship between high- and intermediate-velocity cloud complexes controversial. This metallicity difference could apparently be explained if IVCs were HVCs at later stages of the HVC – disc collision. The clouds would then have accreted a large amount of Galactic matter. From numerical simulations, however, remains unclear the extent to which such gas-mixing in cloud cores can occur (e.g. Santillán et al 1999, but see also Vieser 2001).

A more detailed discussion of the properties of IVCs and HVCs, would require not only knowledge of the probability with which a particular Gaussian belongs to a intermediate- or high-velocity gas cloud, but a full identification of structures in position – position – velocity – line width space.

Acknowledgements. The author would like to thank W. B. Burton for providing the preliminary data from the LDS for program testing prior the publication of the survey. A considerable part of the work on creating the decomposition program was done during the stay of U. Haud at the Radioastronomical Institute of Bonn University (now Argelander-Institut für Astronomie). The hospitality of the staff members of the Institute is greatly appreciated. We thank the anonymous referee and the A&A editor M. Walmsley for fruitful discussions and considerable help. The project was supported by the Estonian Science Foundation grant no. 6106.

References

- Albert, C. E. & Danly, L. 2004, Intermediate-Velocity Clouds, In High-Velocity Clouds, ed. H. van Woerden, B. P. Wakker, U. J. Schwarz, & K. de Boer, Astrophysics and Space Science Library, vol. 312, 73
- Bajaja, E., Arnal, E. M., Larrarte, J. J., et al. 2005, A&A, 440, 767
- de Heij, V., Braun, B. & Burton, W. B. 2002, A&A, 391, 159
- Habing, H. J. 1966, Bull. Astron. Inst. Netherlands, 18, 323
- Hartmann, L. 1994, The Leiden/Dwingeloo Survey of Galactic Neutral Hydrogen, Ph. D.-Thesis, Leiden Univ.
- Haud, U. 1992, MNRAS, 257, 707
- Haud, U. 2000, A&A, 364, 83 (Paper I)
- Haud, U., & Kalberla, P. M. W. 2006, Balt. Astron., 15, 413 (Paper II)
- Haud, U., & Kalberla, P. M. W. 2007, A&A, 466, 555 (Paper III)
- Hulsbosch, A. N. M., & Wakker, B. P. 1988, A&AS, 75, 191
- Kalberla, P. M. W., Burton, W. B., & Hartmann, D., et al. 2005, A&A, 440, 775
- Kalberla, P. M. W., & Haud, U. 2006, A&A, 455, 481
- Kerp, J., Mack, K.-H., Egger, R., et al. 1996, A&A, 312, 67
- Kerp, J., Burton, W. B., Egger, R., et al. 1996, A&A, 342, 213
- Kuntz, K. D., & Danly, L. 1996, ApJ, 457, 703
- Mebold, U. 1972, A&A, 19, 13
- Morras, R., Bajaja, E., Arnal, E. M., & Pöppel, W. G. L. 2000, A&AS, 142, 25
- Santillán, A., Franco, J., Martos, M. & Kim, J. 1999, ApJ, 515, 657
- Schwarz, U. J., & Wakker, B. P. 2004, The Large- and Small-Scale Structure of HVCs, In High-Velocity Clouds, ed. H. van Woerden, B. P. Wakker, U. J. Schwarz, & K. de Boer, Astrophysics and Space Science Library, vol. 312, 145
- Stark, A. A., Gammie, C. F., Wilson, R. W., et al. 1992, ApJS, 79, 77
- Verschuur, G. L. 1975, ARA&A, 13, 257
- Vieser, W. 2001, Ph.D. thesis, Universität Kiel
- Wakker, B. P. 1991, A&A, 250, 499
- Wakker, B. P. 2001, ApJS, 136, 463
- Wakker, B. P. 2004, HVC/IVC Maps and HVC Distribution Function, In High-Velocity Clouds, ed. H. van Woerden, B. P. Wakker, U. J. Schwarz, & K. de Boer, Astrophysics and Space Science Library, vol. 312, 25
- Wakker, B. P., & van Woerden, H. 1997, ARA&A, 35, 217
- Wakker, B. P., de Boer, K. S. & van Woerden, H. 2004, History of HVC Research – An Overview, In High-Velocity Clouds, ed. H. van Woerden, B. P. Wakker, U. J. Schwarz, & K. de Boer, Astrophysics and Space Science Library, vol. 312, 1
- Westphalen, G. 1997, Ph.D.-Thesis, Bonn Univ.